

Reliability assessment for blood oxygen saturation levels measured with optoacoustic imaging

Leonie Ulrich
Kai Gerrit Held
Michael Jaeger
Martin Frenz
Hidayet Günhan Akarçay

SPIE.

Leonie Ulrich, Kai Gerrit Held, Michael Jaeger, Martin Frenz, Hidayet Günhan Akarçay,
“Reliability assessment for blood oxygen saturation levels measured with optoacoustic imaging,”
J. Biomed. Opt. **25**(4), 046005 (2020), doi: 10.1117/1.JBO.25.4.046005

Reliability assessment for blood oxygen saturation levels measured with optoacoustic imaging

Leonie Ulrich,^a Kai Gerrit Held,^{a,b} Michael Jaeger,^a Martin Frenz,^{a,*} and Hidayet Günhan Akarçay^a

^aUniversity of Bern, Institute of Applied Physics, Biomedical Photonics, Bern, Switzerland

^bABB Switzerland, Corporate Research, Baden-Daettwil, Switzerland

Abstract

Significance: Quantitative optoacoustic (OA) imaging has the potential to provide blood oxygen saturation (SO₂) estimates due to the proportionality between the measured signal and the blood's absorption coefficient. However, due to the wavelength-dependent attenuation of light in tissue, a spectral correction of the OA signals is required, and a prime challenge is the validation of both the optical characterization of the tissue and the SO₂.

Aim: We propose to assess the reliability of SO₂ levels retrieved from spectral fitting by measuring the similarity of OA spectra to the fitted blood absorption spectra.

Approach: We introduce a metric that quantifies the trends of blood spectra by assigning a pair of spectral slopes to each spectrum. The applicability of the metric is illustrated with *in vivo* measurements on a human forearm.

Results: We show that physiologically sound SO₂ values do not necessarily imply a successful spectral correction and demonstrate how the metric can be used to distinguish SO₂ values that are trustworthy from unreliable ones.

Conclusions: The metric is independent of the methods used for the OA data acquisition, image reconstruction, and spectral correction, thus it can be readily combined with existing approaches, in order to monitor the accuracy of quantitative OA imaging.

© The Authors. Published by SPIE under a Creative Commons Attribution 4.0 Unported License. Distribution or reproduction of this work in whole or in part requires full attribution of the original publication, including its DOI. [DOI: [10.1117/1.JBO.25.4.046005](https://doi.org/10.1117/1.JBO.25.4.046005)]

Keywords: quantitative optoacoustic imaging; spectral correction; spectral fit; metric; goodness of fit.

Paper 200007R received Jan. 8, 2020; accepted for publication Mar. 25, 2020; published online Apr. 22, 2020.

1 Introduction

Estimating oxygen levels in blood is of paramount importance in various preclinical and clinical applications, e.g., for the study of tumor characteristics,^{1,2} personalized cancer treatment,^{3–6} or the detection and monitoring of cerebral ischemia in newborns.^{7,8} Quantitative optoacoustic (OA) imaging is an emerging technique that allows the determination of blood oxygen saturation (SO₂) by exploiting the distinct absorption spectra of oxy- and deoxyhemoglobin^{9,10} while providing a higher spatial resolution in deep tissue than diffuse optical tomography.^{11,12} The estimation of SO₂ levels can be achieved by performing spectral fits of blood absorption spectra to measured OA spectra, after correcting them for spectral distortions induced by the wavelength-dependent attenuation of light in tissue.^{9,13,14} One major aspect that has recently gained increasing attention is assessing the reliability of the quantitative results.^{15,16} In this paper, we focus on estimating the uncertainty of the SO₂ levels retrieved from spectral fitting, independently of the methods used for OA data acquisition, image reconstruction, or for the correction of spectral distortions. More precisely, we dwell on the fact that fitted SO₂ values that are physiologically

*Address all correspondence to Martin Frenz, E-mail: martin.frenz@iap.unibe.ch

reasonable do not necessarily imply that the measured OA spectra follow the trend of real blood spectra. Determining the uncertainty of a fit is a notoriously difficult task that cannot be solved by generally applicable methods.^{17–20}

We propose to assess the trustworthiness of the SO_2 values by evaluating the similarity between the trends of the measured OA spectra and the trends of the fitted blood spectra. To quantify the spectral trends, we introduce a metric based on the distinctive shape of blood spectra. With the examples of an artery and a vein in a human forearm, we showcase how this metric can be applied to quantitative OA imaging *in vivo*. The measurements were performed using a handheld OA system with a linear array ultrasound (US) transducer, acquiring two-dimensional (2-D) cross-sectional images of the forearm. We start by identifying and analyzing the distorted OA spectra that originate from the vessels of interest, which constitutes an essential part of the quantitative analysis of OA images. For spectral correction, we use multiple irradiation sensing (MIS) that has been described in detail elsewhere.^{21–24} After spectral correction, we determine the SO_2 levels in the vessels and assess the reliability of the outcomes using the metric.

2 Materials and Methods

2.1 Experimental Setup and Data Acquisition

We performed OA experiments on the inside of the forearm of a healthy volunteer, close to the wrist, to determine the SO_2 in the median artery located at a depth of $z \approx 12$ mm and in a side branch of the median antebrachial vein at $z \approx 8$ mm, see Fig. 1(a). The experiments were done in compliance with the ethical principles of the Declaration of Helsinki (2018). The OA system used has been described in detail in Ref. 24. In short, we illuminated the tissue using a diode-pumped Q-switched Nd:YAG laser (Spotlight DPSS OPO, InnoLas Laser GmbH, Germany) with integrated optical parametric oscillator. The light was coupled into a multimode fiber (Thorlabs), which was fixed on a motorized translation stage (T-series, Zaber, Canada), allowing an automated stepwise translation of the irradiation spot. For OA signal detection, we employed a linear array US probe (ATL L7-4, Philips N.V., The Netherlands) connected to a research US system (V1-64, Verasonics). The transducer was placed on the forearm, the linear array being oriented perpendicularly to the longitudinal axis y of the arm, defining $y = 0$ [see Figs. 1(a) and 1(b)]. The arm was immobilized by an arm holder to reduce motion artifacts.²⁵ US gel was used for acoustic coupling between the transducer and the skin. While acquiring real-time OA and US images, the position of the transducer was adjusted such that the vessels of interest became visible in the field of view of the transducer. The initial x position of the tip of the illumination fiber, x_1 , was chosen to be directly above the median artery, i.e., to correspond to the minimal distance between the irradiation spot on the skin and the artery. The y position of the fiber tip was kept at

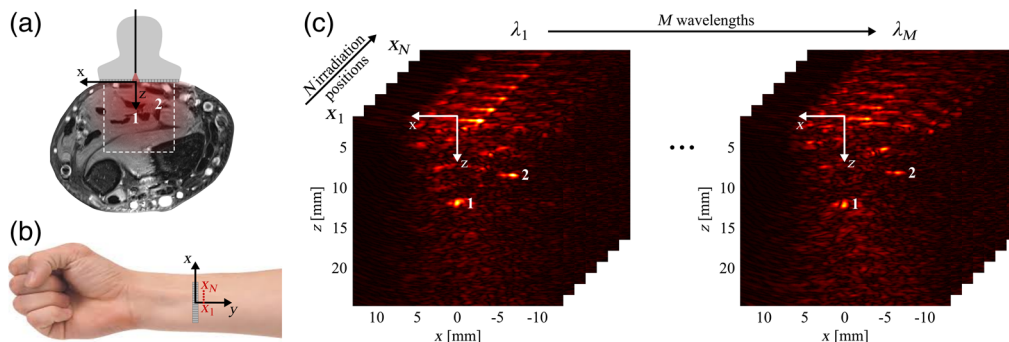


Fig. 1 (a) Sketch (not to scale) of the illumination fiber and US probe on a cross-sectional magnetic resonance image of the volunteer's forearm, displaying the position of the vessels of interest, namely (1) the median artery and (2) a side branch of the median antebrachial vein. (b) Orientation of the linear US transducer array and the irradiation spot, which is translated along x (not to scale). (c) One data set is formed by $N \cdot M$ reconstructed OA images $S_{ij}(\mathbf{r})$, the OA signals of the two vessels of interest are clearly visible.

Table 1 Wavelengths used for OA acquisitions.

j	1	2	3	4	5	6	7
λ_j (nm)	740	760	780	800	830	860	890

$y_0 = 19$ mm. To perform an MIS acquisition sequence (see [Supplementary Material](#)), the fiber tip was translated along the x axis with a step size of 0.5 mm, over a total distance of 9.5 mm, resulting in $N = 20$ different irradiation spot positions x_i , $i \in \{1, \dots, N\}$ [see Fig. 1(b)]. At each position, 150 OA acquisitions were averaged to increase the signal-to-noise ratio (SNR). The surface of the arm was flat within the range scanned with the irradiation spot position, and the position x_N of the outermost irradiation spot was around 20 mm away from the edge of the arm (top-down view). Therefore, the experimental conditions roughly complied with the assumptions made by the MIS approach with regard to tissue boundaries. The MIS acquisition sequence was repeated for $M = 7$ wavelengths λ_j , $j \in \{1, \dots, N\}$ (see Table 1). The number of wavelengths was chosen as a trade-off between the robustness of the spectral fit and an acceptable acquisition time. Although, in general, a higher number of wavelengths would be desirable, the resulting increase in acquisition time would at the same time have led to increased motion artifacts. The set of wavelengths was chosen so that it contained the isosbestic point at $\lambda_{\text{iso}} \approx 800$ nm (needed for the reliability assessment, see Sec. 2.3), and an equal number (3) of wavelengths left and right of λ_{iso} . To the right of λ_{iso} , the wavelength range was limited by the stability of the laser as well as by a low SNR. To the left, we distributed the three wavelengths to capture the spectral peak around $\lambda = 760$ nm for deoxygenated blood. Overall, we sampled the range between $\lambda = 740$ nm and $\lambda = 890$ nm with wavelengths spaced equidistantly within the wavelength intervals to the left and right of the isosbestic point. A frequency-domain algorithm²⁶ was employed to reconstruct $N \cdot M$ radio-frequency (rf)-mode images with a pixel resolution of $149 \mu\text{m} \times 77 \mu\text{m}$ in the x and z direction, respectively. Further analysis was performed based on the envelopes of these rf-mode images, which will from now on be referred to as OA images and denoted by $S_{ij}(\mathbf{r})$, for irradiation positions x_i and wavelengths λ_j . The signals stemming from the artery and the vein are clearly visible in the OA images [see Fig. 1(c)], in the following they will be called OA signals. To be able to correct for wavelength-dependent variations in laser output, the average pulse energies were recorded for each wavelength λ_j . During the OA measurements, a standard pulse oximeter (Nellcor Oximax NPB-40, Medtronic, Ireland) was used to measure the reference arterial SO_2 of the volunteer.

2.2 Motion Correction, Identification of Support, and Pixelwise SO_2 Determination

Figure 2(a) shows the OA signals recorded from both the artery and the vein, for one irradiation position. Part (a) in the animation (Video 1) reveals that, despite the use of an arm holder for immobilization, the vessel positions fluctuate between different λ_j . To compensate for these fluctuations, we defined the x and z positions of the vessels, (x_{ij}^c, z_{ij}^c) , by manually identifying the centers of the corresponding OA signals in all $N \cdot M$ OA images and subsequently shifted the images such that all (x_{ij}^c, z_{ij}^c) coincide. Part (b) of the animation (Video 1) displays the OA signals after motion correction and confirms that the centers are congruent. However, due to noise and out-of-plane motion, the size, shape, and 2-D profile of the OA signals vary with wavelength, introducing an uncertainty in the analysis of the OA signals. To account for this uncertainty, we perform, for each OA signal, a statistical analysis over the pixels corresponding to the respective vessel. These pixels were identified by employing a simple thresholding method (such as, e.g., in Refs. 27–29), assuming that the intensity of signals originating from vessels significantly exceeds the signal intensity in the background. As a threshold, we chose the pixel intensity that corresponded to $1/e$ of the maximum pixel value within a manually selected region of interest covering the vessel's OA signal. In consistence with the terminology introduced in Ref. 12, we call the selected set of pixels the support, defined as “a set of pixels in which the signal values ... are determined by the optical absorption inside ... [the] vessel”. Figure 2(c)

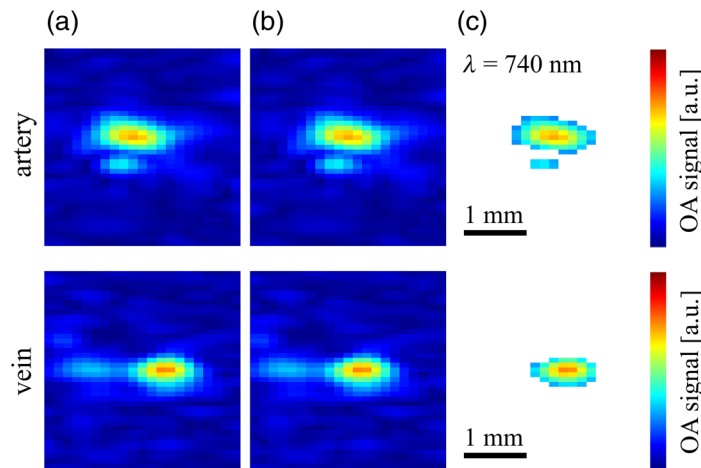


Fig. 2 OA signals emanating from (top) the artery and (bottom) the vein for the different wavelengths λ_j , for one irradiation position, (a) before and (b) after motion correction, together with (c) segmented supports (Video 1, MPEG, 4.5 MB [URL: <https://doi.org/10.1117/1.JBO.25.4.046005.1>]).

shows the supports for both the artery and the vein, for the same OA signals that were presented in Figs. 2(a) and 2(b). Separately for each irradiation position x_i , the pixelwise analysis of the spectra was performed on the subset of pixels that were part of the support for all $M = 7$ wavelengths. The decision to exclude pixels from the analysis was motivated by the following rationale: on the one hand, we did not want to include pixels that—for one or more wavelengths—did not fulfill the criterion for the support, as such pixels were not considered to reliably reflect the absorption of the blood in the vessel. On the other hand, we did not want to include pixels with less than $M = 7$ spectral data points, as 7 is already a very small number with regard to the spectral analysis.

For the pixels that were part of the support for all wavelengths, we performed the analysis of the OA spectra both before and after correction of distortions induced by the wavelength-dependent attenuation of light in the tissue. As mentioned earlier, the spectral correction was achieved by optically characterizing the forearm tissue according to the MIS principle (details on the spectral correction technique are given in the [Supplementary Material](#) and in Video S1, MPEG, 5.3 MB [URL: <https://doi.org/10.1117/1.JBO.25.4.046005.4>] and Video S2, MPEG, 5.6 MB [URL: <https://doi.org/10.1117/1.JBO.25.4.046005.5>]). We determined the effective attenuation coefficient μ_{eff} of the tissue for every wavelength λ_j and analytically calculated the fluences $\Phi_{ij}(\mathbf{r})$ in the OA image plane for x_i and λ_j , with the pixel resolution of the OA images. The spectral correction is then simply a pixelwise division of OA images $S_{ij}(\mathbf{r})$ by $\Phi_{ij}(\mathbf{r})$. Subsequently, SO_2 levels were determined by spectral fitting to the corrected OA spectra, for every individual pixel in the supports.

2.3 Metric for Quantitative Characterization of Spectral Trends

In this section, we address the central issue of this paper, namely the importance of assessing the reliability of the spectral fits. In Fig. 3(a), we have plotted blood absorption spectra in the wavelength range used for the experiments, for SO_2 values between 0% and 100% with a step size of 10%, the respective SO_2 level being indicated in color code. To construct these spectra, we extracted the absorption spectra $\mu_a^{\text{HbO}_2}$ and μ_a^{Hb} of oxy- and deoxyhemoglobin from Ref. 30 and, assuming that hemoglobin is the dominant absorber in blood,³¹ calculated the absorption spectrum of blood at a particular SO_2 as the respective linear combination of $\mu_a^{\text{HbO}_2}$ and μ_a^{Hb} . It can be seen that the blood spectra in Fig. 3(a) follow a range of trends. This range is such that a spectral fit can result in an SO_2 value that can be interpreted as physiologically reasonable, even if the measured OA spectrum is not an actual blood spectrum. We illustrate

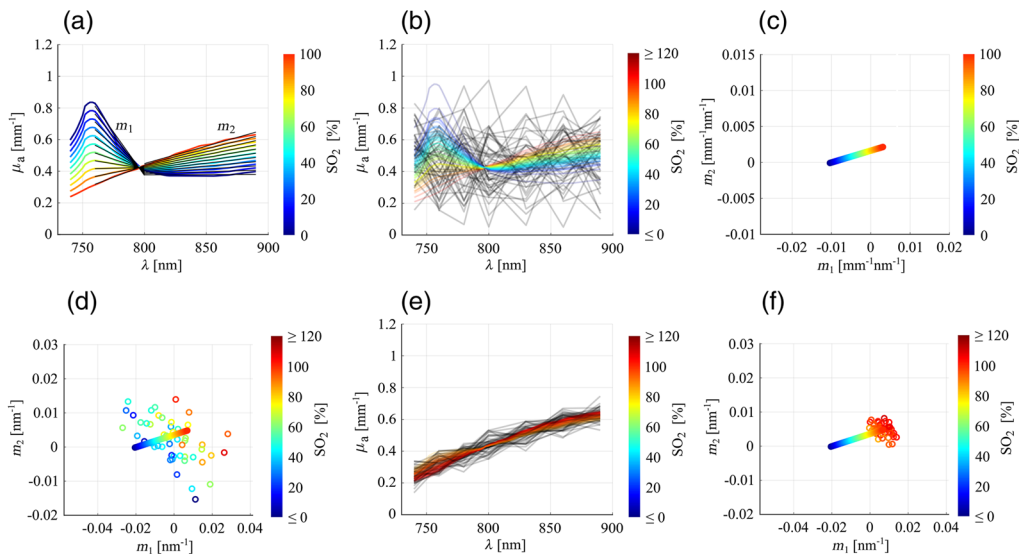


Fig. 3 (a) Blood spectra for SO_2 levels between 0% (blue) and 100% (red), together with the fitted first-order polynomials (in black) to the spectra left and right of the isosbestic point. (b) Synthetic OA spectra (random Gaussian noise, in black) with fitted blood spectra (in color), colors indicating the respective SO_2 levels. (c) Pairs of the two slopes m_1 and m_2 determined for the blood spectra shown in (a), constituting the reference line for the metric plots. (d) Metric plot for the synthetic OA spectra shown in (b): reference line together with slope pairs (m_1 , m_2) determined for the synthetic OA spectra (circles), colors indicate the SO_2 . (e) Synthetic arterial blood spectra (in black), generated by adding random Gaussian noise to the absorption spectrum of blood at $SO_2 = 98\%$, together with fitted spectra (in color), colors indicating the respective SO_2 levels. (f) Metric plot for the spectra shown in (e): reference line together with slope pairs (m_1 , m_2) determined for the synthetic OA spectra (circles), colors indicate the SO_2 . For the visualization of the OA spectra in (b) and (e), each OA spectrum was divided by the scaling factor A given by the respective spectral fit. Further note that the change in units between (c) and (d), (f) is caused by the normalization of the spectra before determining (m_1 , m_2); details are given in the text.

such a situation in Fig. 3(b), where we have generated synthetic OA spectra reflecting random Gaussian noise (black lines, the number of spectra roughly corresponds to the number of pixels we found in one support in this study), to which we fitted blood absorption spectra (colored lines, where the color indicates the fitted SO_2 parameter). For the spectral fit, we determined the blood absorption spectrum in the wavelength range between $\lambda = 740$ nm and $\lambda = 890$ nm that matches the OA data best in the least-squares sense, using the fit function $y(\lambda) = A \cdot [\mu_a^{\text{HbO}_2}(\lambda) \cdot (SO_2/100) + \mu_a^{\text{Hb}}(\lambda) \cdot (1 - SO_2/100)]$ with the SO_2 (in %) and a scaling factor A as fit parameters. Note that the factor A accounts for the fact that the absolute amplitude of a real OA signal detected with a linear array probe does not bear a quantitative meaning as it depends via the system impulse response on the vessel orientation,³² which induces an unknown scaling of OA spectra. Even though the OA spectra shown in Fig. 3(b) are random noise, the corresponding spectral fits result in SO_2 values mostly between 0% and 100%. This highlights that the mere fact that a fit yields a physiologically possible SO_2 value does not necessarily imply that the OA spectrum is well described by the fitted blood spectrum and the SO_2 value is meaningful.

Assessing the reliability of the outcome of a fit is known to be a nontrivial task, which often necessitates *ad hoc* solutions.^{19,33} Standard goodness-of-fit parameters, like, e.g., χ^2 (the sum of squared residuals) or R^2 , have limited suitability for our purpose because they cannot identify whether the differences between the data points and the fitted curve are biased (i.e., systematic). On the other hand, analyzing the quality of the spectral fit using more sophisticated statistical procedures is usually impeded by a very low number of available data points (wavelengths) as a consequence of limits in the acquisition time acceptable for *in vivo* measurements, together with technical constraints of the OA experiment. Instead, we suggest to use a customized method that

is tailored to the analysis of fits of blood spectra and easy to use. More specifically, we propose to determine the similarity between the trend of the measured OA spectrum and the trend of the fitted blood spectrum.

To quantify the trends of blood spectra, we exploit a distinctive feature in the wavelength range between $\lambda = 760$ nm and $\lambda = 890$ nm, namely that the trends of the spectra before and after the isosbestic point at around $\lambda_{\text{iso}} \approx 800$ nm can be approximated by straight lines with slopes m_1 and m_2 , respectively [see black lines in Fig. 3(a)]. We use the slope pair (m_1, m_2) as a metric and determine the values of m_1 and m_2 by performing least-squares fits of two first-order polynomials to the spectra on the left and right sides of the isosbestic point, respectively. While the spectral fit to determine the SO_2 was performed including the full wavelength range between $\lambda = 740$ nm and $\lambda = 890$ nm, the polynomial fits to determine the slopes m_1 and m_2 were performed on the two subsets of wavelengths $\{760 \text{ nm}, 780 \text{ nm}, 800 \text{ nm}\}$ and $\{800 \text{ nm}, 830 \text{ nm}, 860 \text{ nm}, 890 \text{ nm}\}$, respectively. $\lambda = 740$ nm was not included for the polynomial fits as this wavelength is outside the range in which blood spectra are approximately linear, see Fig. 3(a). The pairs (m_1, m_2) corresponding to actual blood with $0\% \leq \text{SO}_2 \leq 100\%$ constitute a reference and are visualized in a scatter plot [m_2 against m_1 , see Fig. 3(c)] as color-filled points, where the color denotes the corresponding SO_2 value, like in Fig. 3(a). It can be seen that the points form a line, in the following called reference line. Likewise, to quantify the trend of a measured OA spectrum, we determine the slope pair (m_1, m_2) by performing least-squares fits of two first-order polynomials to the OA data points left and right of the isosbestic point. Due to the aforementioned unknown scaling of the measured OA spectra, direct fits to the OA spectra would not result in slopes that are comparable to those of actual blood. To obtain (m_1, m_2) values that do not depend on the scaling, we normalized the OA spectra before performing the polynomial fits to determine (m_1, m_2) . We normalized each OA spectrum by dividing it by its respective mean value across the full wavelength range between $\lambda = 740$ nm and $\lambda = 890$ nm. The same normalization was used for a redefinition of the reference line to ensure comparability, i.e., we divided each blood spectrum by the respective mean value over the set of wavelengths used for the OA measurement, before determining the reference slope pairs (m_1, m_2) . Note that this normalization causes a change in magnitude and unit of the reference (m_1, m_2) with respect to the original reference line shown in Fig. 3(c). To measure the similarity between the trend of a measured OA spectrum and the trend of the blood spectrum determined in the corresponding spectral fit, the slope pair (m_1, m_2) for the OA spectrum is visualized as a colored circle in the scatter plot together with the reference line (the color of the circle designating the SO_2 level given by the spectral fit). The resulting scatter plot containing the reference line and the circles for all OA spectra in the support, referred to as metric plot, allows one to assess the reliability of the spectral fits.

We illustrate this with two examples. In the first example in Fig. 3(d), the position of each circle represents the pair (m_1, m_2) for one of the synthetic OA spectra given in Fig. 3(b). The positions of the circles mostly far away from the reference line indicate that no systematic similarity can be established between the trends of the OA spectra and those of the fitted spectra, meaning that the fits, even though they may result in physiologically possible SO_2 values, are not trustworthy. In case of a high similarity between the trends of measured OA spectra and the trends of fitted blood spectra, each colored circle would be close to the respective point in the reference line having the same color. Such a situation is illustrated with a second example, see Figs. 3(e) and 3(f). Figure 3(e) shows synthetic OA spectra (black lines) for an artery, numerically generated by adding random Gaussian noise to the absorption spectrum of blood at $\text{SO}_2 = 98\%$ (which is a typical SO_2 level for arterial blood³⁴). The SNR was adjusted to be comparable to that observed in our OA images. Again, the number of spectra was chosen to roughly correspond to the number of pixels we obtained in a support. The red color of the fitted blood spectra indicates that the reference SO_2 (98%) has been retrieved correctly. The corresponding metric plot is given in Fig. 3(f). Two main observations can be made. First, the circles describing the trends of the OA spectra across the support are clustered, which contrasts with the situation given in Fig. 3(d). This means that we can identify a systematic trend, i.e., the trends of OA spectra do not differ much between individual pixels, despite the stochastic fluctuations in the spectra. Note that a statistically meaningful number of spectra, provided by the pixelwise analysis in a support, is a prerequisite for the identification of a cluster in the

corresponding metric plot. Second, the position of the cluster agrees with the position of the points on the reference line covering the same color range. These two observations together indicate that the trends of the OA spectra do indeed systematically resemble the trends of the fitted blood spectra. The metric plot combines all the relevant information needed to comprehensively represent the outcomes of an SO_2 estimation, namely (i) information on the uniformity of the spectral trends across the support (clustering of circles), (ii) the fitted SO_2 values across the support (colors of circles), and (iii) information on the similarity between the OA spectra and the fitted blood spectra (proximity of circles to points on the reference line covering the same color range).

3 Results and Discussion

3.1 Quantitative Analysis of Uncorrected OA Spectra

In a first step, we would like to demonstrate based on our *in vivo* data that the metric can already be used to quantitatively analyze the measured OA spectra before correction. The analysis of uncorrected spectra can be helpful as, in case of an unsuccessful spectral correction, it would be difficult to distinguish potential sources of error related to the different steps involved in the analysis if merely the corrected OA spectra were investigated. In particular, applying a spectral correction and determining SO_2 levels is only sensible if one is certain that the corresponding supports have been correctly identified and that motion artifacts have been corrected for. We show that this can be ascertained using parts of the information given in the metric plots, namely by observing the clustering of slope pairs.

Figures 4(a) and 4(b) show the uncorrected OA spectra (black lines) for all pixels within the supports for the artery and the vein, respectively, for one irradiation position. According to the definition of the support (recall Sec. 2.2), every pixel in the support is assumed to reflect the wavelength dependency of the total energy absorbed in the corresponding vessel and thus the OA spectra are expected to be uniform across the support. This assumption is reasonable if either (i) the optical penetration depth is much larger and/or (ii) the vessel diameter is much smaller than the size of the point spread function of the imaging system.³⁵ In this study, the first condition is roughly fulfilled [the size of the point spread function is ~ 0.5 mm and the penetration depth is around 2 mm ($\mu_a \approx 0.5$ mm⁻¹)] and, in agreement with the expectation, the spectra corresponding to individual pixels of one support are relatively uniform, both for the artery and the vein. The small variations observed between individual spectra are a result of differences in the size, shape, and 2-D profile of the supports that occurred between the acquisitions of data sets corresponding to different wavelengths (recall Sec. 2.2). The variations are slightly larger for the vein due to

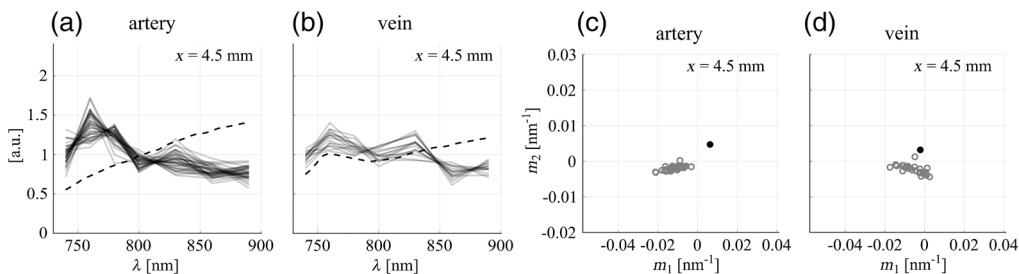


Fig. 4 (a), (b) Uncorrected OA spectra corresponding to individual pixels within the support (black lines), for the artery and the vein, respectively. Reference blood spectra are shown as dashed lines and correspond to the reference SO_2 level determined by pulse oximetry ($\text{SO}_2 = 98\%$) and an average literature value ($\text{SO}_2 = 70\%$), respectively. For the visualization, each uncorrected OA spectrum and reference blood spectrum was normalized by dividing it by its respective mean value over the set of wavelengths used for the OA measurement. (c), (d) Reduced metric plots for spectra shown in (a), (b), pairs (m_1, m_2) determined for the OA spectra are shown as gray circles, (m_1, m_2) for the reference blood spectra are given as black points. A video showing the figure for all x_i is available (Video 2, MPEG, 8.4 MB [URL: <https://doi.org/10.1117/1.JBO.25.4.046005.2>]).

a lower SNR. Nevertheless, for both the artery and the vein, it can be seen that the spectra follow a systematic trend.

Furthermore, it is apparent in Figs. 4(a) and 4(b) that the trends of the spectra recorded from the artery and the vein are distorted with respect to the actual absorption spectra of the blood in the vessels (dashed lines), due to the wavelength-dependent attenuation of the light. The reference spectra correspond to $\text{SO}_2 = 98\%$ (given by the pulse oximeter measurement) for the artery and to $\text{SO}_2 = 70\%$ (average literature value^{36–38}) for the vein. Interestingly, the OA spectra are very similar to blood spectra at low SO_2 levels [compare Fig. 3(a)]. However, this similarity is not relevant as for vessels located at these depths in the tissue, the spectral distortion is generally expected to be significant and thus uncorrected OA spectra most likely do not represent the actual absorption spectra of the blood in the vessels. In fact, spectral fits to the uncorrected OA spectra shown in Figs. 4(a) and 4(b) result in unphysiologically low SO_2 values, i.e., around 20% for the artery and 30% for the vein.

The qualitative observations in Figs. 4(a) and 4(b) are summarized in a condensed way in a reduced representation of the metric plot. Since, as mentioned above, before correction there is generally no reason to expect that the trends of the OA spectra follow the ones of actual blood, a comparison between the positions of the slope pairs and the reference line [as it was done in Figs. 3(d) and 3(f)] is not meaningful. Hence, the reduced metric plot does not include information on fitted SO_2 levels and omits the reference line. In Figs. 4(c) and 4(d), the reduced metric plots are given for the spectra shown in Figs. 4(a) and 4(b), respectively. The existence of systematic trends in the measured OA spectra is underlined by a strong clustering of slope pairs (m_1, m_2) both for the artery and the vein, corroborating the good performance of the motion correction and segmentation procedure outlined in Sec. 2.2 and thus confirming that it is sensible to proceed to the spectral correction.

In addition, the reduced metric plots allow one to visualize the distortion of the OA spectra with respect to the reference blood spectra for the artery and the vein. For this purpose, we have added the reference slope pairs (corresponding to $\text{SO}_2 = 98\%$ and $\text{SO}_2 = 70\%$, respectively, displayed as black points). A measure for the spectral distortion is given by the position of the cluster with respect to the position of the reference point: for the artery, the distance between the cluster and the reference point is larger than for the vein, confirming the stronger distortion of the spectra in Figs. 4(a) than in 4(b). The degree of distortion of measured OA spectra is generally expected to depend on the distance between the irradiation spot at the tissue surface and the blood vessel. According to Eq. (1) in the [Supplementary Material](#), given a particular wavelength dependency of μ_{eff} , a larger distance from the illumination source leads to more pronounced differences in the fluence between different wavelengths and thus to a more pronounced spectral distortion. Although the artery is located at a larger depth than the vein, the distance between the irradiation spot and the vessel is, for the irradiation position $x = 4.5$ mm, larger for the vein than for the artery, due to the irradiation geometry used in the experiment. Therefore, the stronger distortion for the artery cannot be explained by the distance from the illumination source. A plausible reason for the observed differences in the distortion of the OA spectra could be differences in the optical properties of the two tissue segments that are located between the skin and the artery/vein.

3.2 Quantitative Analysis of Corrected OA Spectra

After having established the good performance of the motion correction and segmentation procedure, we proceed by showing the results of the spectral correction.

Figure 5 displays the spectra of the effective attenuation coefficient (μ_{eff}) used for the correction of the OA spectra. According to the MIS approach, the μ_{eff} spectrum assigned to each blood vessel is expected to optically characterize a tissue segment for which the diffusion approximation is valid (see [Supplementary Material](#)). Since these two tissue segments differ (they are defined by different subsets of irradiation positions at the forearm surface and different positions of the vessels, see [Supplementary Material](#)), they might have different optical properties. This is a possible explanation for the significant difference between the μ_{eff} obtained for the artery and the vein. For both tissue segments, the μ_{eff} spectra are in line with the broad range of effective attenuation coefficients of human tissue reported in the literature (approximately

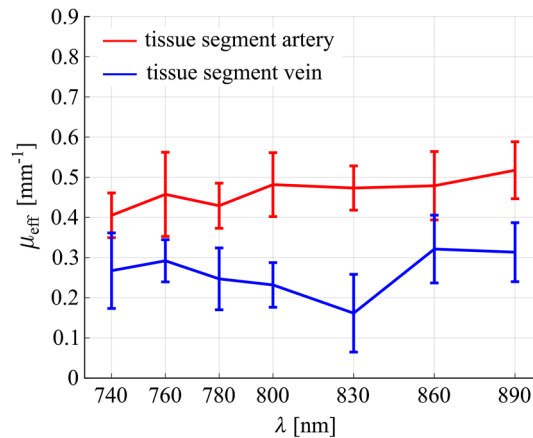


Fig. 5 μ_{eff} spectra estimated for the tissue between the irradiation points at the forearm surface and the artery (red) and the vein (blue).

between 0.1 and 1 mm $^{-1}$).^{39–43} Note that, for both the artery and the vein, spectral correction was only performed for the respective subset of irradiation positions corresponding to the tissue segment that is optically characterized by the μ_{eff} given in Fig. 5.

The OA spectra retrieved after correction are shown as black lines in Figs. 6(a) and 6(b), for the artery and the vein, respectively, together with the blood spectra determined by the spectral fits. It can be clearly seen that the corrected OA spectra exhibit strong fluctuations across the wavelength range. It is reasonable to assume that parts of these fluctuations can be explained by errors in μ_{eff} : it can be observed, by looking at Fig. 5, that fluctuations in the μ_{eff} spectra, although they are less pronounced, are very similar to the fluctuations in the corrected OA spectra. This observation is plausible if one assumes that the observed fluctuations in μ_{eff} are due to measurement errors relative to true μ_{eff} spectra that are much smoother than the measured μ_{eff} spectra. Such errors would indeed appear in the corrected OA spectra, because, as explained in Sec. 2.2, μ_{eff} is used to calculate the fluence $\Phi_{ij}(\mathbf{r})$, and the corrected OA spectra are determined by performing a division of the OA image $S_{ij}(\mathbf{r})$ by the fluence $\Phi_{ij}(\mathbf{r})$. Due to the exponential dependence of the fluence on μ_{eff} [see Eq. (1) in the [Supplementary Material](#)], errors in the μ_{eff} spectra appear in an amplified way in the corrected OA spectra.

As mentioned earlier, the goal of this paper is to demonstrate the necessity of assessing the reliability of spectral fits. Qualitatively, it can be seen in Figs. 6(a) and 6(b) that, for the vein, the level of fluctuations in the OA spectra around the fitted blood spectra is larger than for the artery. This can already be regarded as an indication of a difference in the reliability of the spectral correction between the artery and the vein, and one could, e.g., attempt to quantify the reliability based on χ^2 , which would represent a measure for the level of fluctuations in the OA spectra. With regard to the reliability assessment of the SO_2 estimation, however, the level of fluctuations is not the main deciding factor. We argue that the more fundamental question is to what extent the corrected OA spectra have a systematic trend that resembles that of actual blood. As already explained in Sec. 2.3, simply fitting blood spectra to the corrected OA spectra can be misleading: the SO_2 values corresponding to the fitted blood spectra in Figs. 6(a) and 6(b) (indicated in color) are physiologically realistic both for the artery (fitted SO_2 values around 100%) and the vein (fitted SO_2 values around 60%). For the artery, it can be seen that the OA spectra fluctuate around the monotonically increasing blood spectra determined by the spectral fits, whereas a substantial deviation in the trends between OA spectra and fitted spectra can be observed for the vein. To quantify this qualitative observation, we use the metric introduced in Sec. 2.3, as it provides a measure to quantify the agreement between spectral trends that is—as we argue—more relevant for the SO_2 . The metric plots corresponding to the corrected OA spectra shown in Figs. 6(a) and 6(b) are given in Figs. 6(c) and 6(d), respectively. For the artery, the colored circles are clustered close to the filled points on the reference line covering the same color range. This underlines that the corrected OA spectra systematically follow the trends of the fitted blood spectra [both observations stated in Sec. 2.3 are fulfilled, like in the example shown in Fig. 3(f)] and attests the

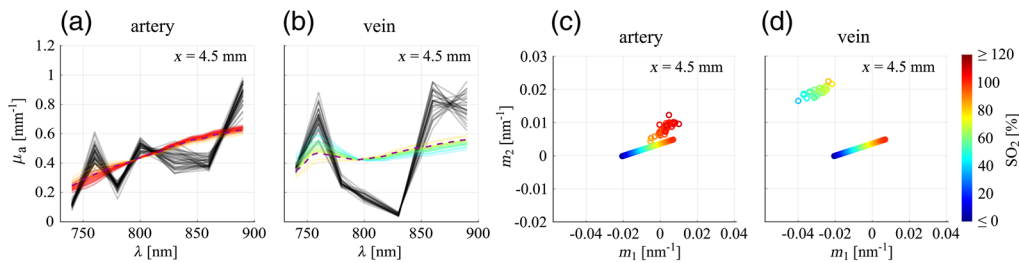


Fig. 6 (a), (b) Corrected OA spectra corresponding to individual pixels within the support (black lines), for the artery and the vein, respectively, together with the fitted spectra that are plotted in color to indicate the respective SO_2 levels. For the visualization, each OA spectrum was divided by the scaling factor A given by the respective spectral fit. Reference spectra are shown as purple dashed lines and correspond to the reference SO_2 level determined by pulse oximetry ($\text{SO}_2 = 98\%$) and an average literature value ($\text{SO}_2 = 70\%$), respectively. (c), (d) Metric plots for spectra shown in (a), (b), representing the reference line together with the pairs (m_1, m_2) determined for the corrected OA spectra. A video showing the figure for all x_i is available (Video 3, MPEG, 7.7 MB [URL: <https://doi.org/10.1117/1.JBO.25.4.046005.3>]).

trustworthiness of the fits (note here that we interpret the cluster's distance from the reference line in relation to its spread: for the artery, the distances of the circles from the reference line are smaller than or comparable to the extent of the cluster). Moreover, the proximity of the cluster to the point on the reference line corresponding to $\text{SO}_2 = 98\%$ indicates a reasonable spectral correction, as the cluster is located closer to the reference point than before correction. For the vein, the circles are also clustered, however, their positions are way off the positions of the points on the reference line covering the same color range, which is a clear indication that the fits are not reliable and that the fitted SO_2 levels, although they are physiologically realistic, are not to be trusted. Here, the erroneous nature of the spectral correction is *de facto* proven without the need of a reference SO_2 , as the distance between the cluster and the reference line in the metric plot reveals the dissimilarity between the corrected OA spectra and actual blood spectra.

Based on these metric plots, it is also possible to quantify a cluster's distance from the reference line in relation to its spread, in order to provide a number that indicates the similarity between the trends of the corrected OA spectra and the trends of the fitted blood spectra. A possible approach to measure the distance of the cluster from the reference line is by determining the mean value of the distances of individual circles in the cluster from the point on the reference line that corresponds to the average SO_2 in the cluster. An approximate measure for the spread of the cluster is, e.g., given by the mean distance of the individual circles from the centroid of the cluster. In the ideal case where the cluster's centroid coincides with the reference point, the ratio between these two quantities would be 1. In this study, we obtain a ratio of 1.71 ± 0.31 for the artery (mean and standard deviation over all irradiation positions) and a ratio of 7.84 ± 3.58 for the vein. The ratio obtained for the artery is thus close to the ideal case, underlining the accuracy of the correction of the artery's OA spectra, whereas the one obtained for the vein is much larger. With regard to a clinical application, one could define a threshold for the aforementioned ratio to identify unreliable results. However, the definition of such a threshold would require more statistics than we can provide, depends on the clinical target, and was therefore beyond the scope of this paper.

From the observed dissimilarity between the corrected OA spectra and actual blood spectra in case of the vein, it can be concluded that the μ_{eff} spectrum given in Fig. 5 for the tissue segment between the irradiation points at the forearm surface and the vein is not trustworthy. A possible reason for the unsuccessful spectral correction for the vein is the fact that the tissue segment that is optically characterized using the MIS method, i.e., the segment between the irradiation points and the vessel, is located in a shallower tissue region than in the case of the artery. For the accuracy of the MIS method, the structure of the tissue that lies between the source and the vessel is crucial. In particular, MIS relies on the assumption that there exist prevalent tissue regions between the irradiation positions and the vessel that can be modeled as an optically quasihomogeneous medium in which the fluence can be described by the analytical diffusion approximation for a semi-infinite medium. This assumption seems to be more violated in case of

the vein, which is plausible, on the one hand, as the photon paths are influenced more strongly by superficial tissue layers, which are likely to have more pronounced optical inhomogeneities, and on the other hand, due to the presumably stronger influence of the boundary (skin surface). It should be noted that we did not comment on the accuracy of the μ_{eff} spectra earlier, as neither a reference for the optical properties is available nor had the performance of the MIS method been validated *in vivo*. The metric analysis proposed in this paper—or any method that allows one to assess the trustworthiness of spectral fits—could be a promising approach to systematically investigate the range of applicability and validity of the MIS method; however, this was not within the scope of this study.

When comparing Figs. 4(a), 4(b) and 6(a), 6(b) with the blood absorption spectra shown in Fig. 3(a), it can be observed that the OA spectra are more similar to actual blood spectra before spectral correction than after correction. However, as mentioned in Sec. 3.1, this observation is not meaningful, as in this tissue depth a substantial spectral distortion is expected and the uncorrected OA spectra therefore in general do not reflect the absorption spectra of the blood in the vessels. Ideally, it would be expected that a spectral correction brings the trends of the OA spectra closer to the spectral trends of the blood in the vessels. However, errors in the estimated μ_{eff} spectra propagate into the corrected OA spectra, and in case of the vein, errors in μ_{eff} led to a dissimilarity between the corrected OA spectra's trends and the spectral trend of actual blood. We would like to underline that it is exactly the goal of the proposed metric to identify such cases. In particular, the *in vivo* results presented in this section highlight what has been mentioned in Sec. 2.3, namely that it is not sufficient to rely on the physiological plausibility of SO_2 values retrieved from spectral fits. We would like to emphasize again that the reliability assessment based on our metric is independent of the technique employed for spectral correction.

The central message of this paper is that in quantitative OA imaging, an assessment of the reliability of spectral fits is advisable, and we suggest that quantifying the similarity between trends of OA spectra and trends of fitted blood spectra constitutes a valuable approach. To showcase this, we proposed a metric on which this similarity analysis can be based. The choice of the particular metric was based on an important observation: in Figs. 3(a) and 3(c), it could be seen that the SO_2 is related to the slopes of the blood spectrum left and right of the isosbestic point in that the slope pairs (m_1, m_2) corresponding to actual blood are uniquely linked to the SO_2 [see reference line in Fig. 3(c)]. One can think of a spectral fit as the characterization of the trend of a blood spectrum with only one free parameter (the SO_2), whereas the metric characterizes the trend of a spectrum in two dimensions $(m_1 \text{ and } m_2)$, thus providing a more detailed description of the trend. In general, a measurement outcome can only be deemed reliable, if alternative methods yield similar results. In our case, we compare the trend that is given by (m_1, m_2) with the trend suggested by the SO_2 resulting from the spectral fit. The two methods are in agreement, if the cluster in the metric plot is located close to the points on the reference line covering the same color range. The proposed metric is sensitive to systematic biases between OA spectra and fitted spectra. The type of bias the metric detects (dissimilarities in the slopes of the spectra left and right of the isosbestic point) is highly relevant with regard to the SO_2 since, as mentioned above, the SO_2 level and the slopes are strongly correlated. Yet, it is important to mention that our metric is very likely not the only metric suitable for the purpose, i.e., for quantifying the similarity between measured and fitted spectra. Another potential approach to quantify the similarity would, e.g., be to apply principle component analysis to both the OA spectra and the fitted blood spectra. It was, however, beyond the scope of this paper to perform a detailed study on the optimal choice of the metric.

4 Conclusion

A central challenge in *in vivo* quantitative OA imaging is the validation of the SO_2 values retrieved in vessels, following the optical characterization of the tissue and the spectral correction of the measured OA spectra that were initially distorted due to the wavelength-dependent optical attenuation of light. Throughout this paper, we have shown that one valuable piece of information that is directly available from the OA measurements is the trends of the OA spectra in the vessel supports, and not only after the spectral correction but also before. The intention is, before

spectral correction, to identify systematic trends of spectra in the supports and, after correction, to assess the similarity between the trends of the corrected OA spectra and those of the fitted blood spectra. This two-step analysis can be extremely helpful to distinguish errors in the measurements and/or image analysis (e.g., imperfect support segmentation, influence of motion artifacts, or a low SNR) from an erroneous spectral correction (i.e., incorrect optical characterization of the tissue). With the examples of *in vivo* measurements from a human artery and vein, we have demonstrated that the analysis of the trends is essential: retrieving physiologically sound SO_2 values does not necessarily indicate that the spectral correction has been successful. In particular, the OA measurements acquired from the vein illustrate a case in which the SO_2 retrieved after correction could misleadingly indicate a successful correction and the metric can be used to disprove this, by showing that the trends of the corrected OA spectra do not agree with the trends of the fitted blood spectra.

The main focus of this paper was to draw attention to the fact that analyzing the similarity between the OA spectra and the fitted blood spectra constitutes an easy way of assessing the reliability of spectral fits. The metric used in this study to quantify spectral trends was chosen with the goal to provide a representative similarity measure that is relevant for the SO_2 . It can easily be incorporated into existing quantitative OA approaches since the analysis is computationally very lightweight and does not need *a priori* knowledge. With the corresponding metric plots, we have introduced a concise representation of the results. These metric plots contain information across the supports on (i) the uniformity of the trends of the OA spectra (this could, in principle, be adapted to perform an automated segmentation of the OA images), (ii) the fitted SO_2 levels, and (iii) the similarity between the OA spectra and the fitted blood spectra. In recent years, promising developments have taken place in the field of quantitative OA imaging (see, e.g., Refs. 44–47) and our metric analysis complements these so as to move forwards with the generation of more reliable medical images.

Disclosures

The authors declare that there are no conflicts of interest related to this article.

Acknowledgments

The authors would like to thank Olivier Scheidegger from the University Hospital Bern for providing the magnetic resonance images of the forearm and for helpful discussions. This work has been funded by the Swiss National Science Foundation under project no. 205320_179038. All data are available on request from the corresponding author.

References

1. D. W. Siemann, “The unique characteristics of tumor vasculature and preclinical evidence for its selective disruption by tumor-vascular disrupting agents,” *Cancer Treat. Rev.* **37**(1), 63–74 (2011).
2. J. C. Forster et al., “A review of the development of tumor vasculature and its effects on the tumor microenvironment,” *Hypoxia* **5**, 21–32 (2017).
3. P. Okunieff et al., “Tumor oxygen measurements and personalized medicine,” in *Oxygen Transport to Tissue XXXIV*, Advances in Experimental Medicine and Biology, W. J. Welch et al., Eds., Vol. **765**, pp. 195–201, Springer, New York (2013).
4. J. C. Walsh et al., “The clinical importance of assessing tumor hypoxia: relationship of tumor hypoxia to prognosis and therapeutic opportunities,” *Antioxid. Redox Signaling* **21**(10), 1516–1554 (2014).
5. D. Vordermark and M. R. Horsman, “Hypoxia as a biomarker and for personalized radiation oncology,” in *Molecular Radio-Oncology*, Recent Results in Cancer Research, M. Baumann, M. Krause, and N. Cordes, Eds., Vol. **198**, pp. 123–142, Springer, Berlin, Heidelberg (2016).

6. F. Colliez, B. Gallez, and B. F. Jordan, "Assessing tumor oxygenation for predicting outcome in radiation oncology: a review of studies correlating tumor hypoxic status and outcome in the preclinical and clinical settings," *Front. Oncol.* **7**, 10 (2017).
7. S. Badurdeen et al., "Haemodynamic instability and brain injury in neonates exposed to hypoxia-ischaemia," *Brain Sci.* **9**(3), 49 (2019).
8. M. Dehaes et al., "Cerebral oxygen metabolism in neonatal hypoxic ischemic encephalopathy during and after therapeutic hypothermia," *J. Cereb. Blood Flow Metab.* **34**(1), 87–94 (2014).
9. B. Cox et al., "Quantitative spectroscopic photoacoustic imaging: a review," *J. Biomed. Opt.* **17**(6), 061202 (2012).
10. J. Xia, J. Yao, and L. V. Wang, "Photoacoustic tomography: principles and advances," *Electromagn. Waves* **147**, 1–22 (2014).
11. A. Puszka et al., "Spatial resolution in depth for time-resolved diffuse optical tomography using short source-detector separations," *Biomed. Opt. Express* **6**(1), 1–10 (2015).
12. L. Ulrich et al., "Spectral correction for handheld optoacoustic imaging by means of near-infrared optical tomography in reflection mode," *J. Biophotonics* **12**(1), e201800112 (2019).
13. B. T. Cox, J. G. Laufer, and P. C. Beard, "The challenges for quantitative photoacoustic imaging," *Proc. SPIE* **7177**, 717713 (2009).
14. M. Li, Y. Tang, and J. Yao, "Photoacoustic tomography of blood oxygenation: a mini review," *Photoacoustics* **10**, 65–73 (2018).
15. J. Gröhl et al., "Confidence estimation for machine learning-based quantitative photoacoustics," *J. Imaging* **4**(12), 147 (2018).
16. N. Hänninen, A. Pulkkinen, and T. Tarvainen, "Image reconstruction with reliability assessment in quantitative photoacoustic tomography," *J. Imaging* **4**(12), 148 (2018).
17. W. Guthrie, A. Filliben, and T. Tarvainen, "NIST/SEMATECH e-handbook of statistical methods," in *Process Modeling* (2013).
18. J. Martin, D. D. R. de Adana, and A. G. Asuero, "Fitting models to data: residual analysis, a primer," Chapter 7 in *Uncertainty Quantification and Model Calibration*, J. P. Hessling, Ed., p. 133, INTECHOPEN, London (2017).
19. A. Maydeu-Olivares and C. García-Forero, "Goodness-of-fit testing," in *International Encyclopedia of Education*, 3rd ed., P. Peterson, E. Baker, and B. McGaw, Eds., Vol. **7**, pp. 190–196, Elsevier, Oxford (2010).
20. T. Strutz, "Uncertainty of results," Ch. 4 in *Data Fitting and Uncertainty*, 1st ed., pp. 105–124, Vieweg+Teubner, Wiesbaden, Germany (2011).
21. R. J. Zemp, "Quantitative photoacoustic tomography with multiple optical sources," *Appl. Opt.* **49**(18), 3566–3572 (2010).
22. J. C. Ranasinghesagara, Y. Jiang, and R. J. Zemp, "Reflection-mode multiple-illumination photoacoustic sensing to estimate optical properties," *Photoacoustics* **2**(1), 33–38 (2014).
23. K. G. Held et al., "Spectral correction of OA signals based on multiple irradiation sensing: experimental validation," *Proc. SPIE* **9708**, 97081E (2016).
24. K. G. Held et al., "Multiple irradiation sensing of the optical effective attenuation coefficient for spectral correction in handheld OA imaging," *Photoacoustics* **4**(2), 70–80 (2016).
25. S. Preisser et al., "Study of clutter origin in *in-vivo* epi-optoacoustic imaging of human forearms," *J. Opt.* **18**(9), 094003 (2016).
26. M. Jaeger et al., "Fourier reconstruction in optoacoustic imaging using truncated regularized inverse k-space interpolation," *Inverse Prob.* **23**(6), S51–S63 (2007).
27. D. de Muinck Keizer, "Photoacoustic tomography for finger joint imaging: tackling artefacts," Master Thesis, University of Twente (2017).
28. Z. Li et al., "PA vessel: practical 3D vessel structure sensing through photoacoustic effects with its applications in palm biometrics," *Proc. ACM Interact. Mobile Wearable Ubiquitous Technol.* **2**(3), 122:1–122:24 (2018).
29. P. Raunonen and T. Tarvainen, "Segmentation of vessel structures from photoacoustic images with reliability assessment," *Biomed. Opt. Express* **9**(7), 2887–2904 (2018).
30. S. Prahl, "Optical absorption of hemoglobin," Oregon Medical Laser Center, 1999, <http://omlc.org/spectra/hemoglobin/>.

31. N. Bosschaart et al., “A literature review and novel theoretical approach on the optical properties of whole blood,” *Lasers Med. Sci.* **29**(2), 453–479 (2014).
32. S. Preisser et al., “Vessel orientation-dependent sensitivity of optoacoustic imaging using a linear array transducer,” *J. Biomed. Opt.* **18**(2), 026011 (2013).
33. B. M. Byrne, *Structural Equation Modeling with LISREL, PRELIS, and SIMPLIS: Basic Concepts, Applications, and Programming*, Multivariate Applications Book Series, ch. 3, Lawrence Erlbaum Associates Publishers, Mahwah, New Jersey (1998).
34. J.-A. Collins et al., “Relating oxygen partial pressure, saturation and content: the haemoglobin-oxygen dissociation curve,” *Breathe* **11**(3), 194–201 (2015).
35. M. Sivaramakrishnan et al., “Limitations of quantitative photoacoustic measurements of blood oxygenation in small vessels,” *Phys. Med. Biol.* **52**(5), 1349–1361 (2007).
36. R. M. Pearse and A. Rhodes, “Mixed and central venous oxygen saturation,” in *Yearbook of Intensive Care and Emergency Medicine*, J.-L. Vincent, Ed., pp. 592–602, Springer, New York (2005).
37. H. Schobel, “Mixed venous oxygen saturation,” in *Anesthesiology Core Review, Part II*, B. S. Freeman and J. S. Berger, Eds., p. 13, McGraw-Hill Education. Inc., New York (2016).
38. M. Harms et al., “Postural effects on cardiac output and mixed venous oxygen saturation in humans,” *Exp. Physiol.* **88**(5), 611–616 (2003).
39. S. L. Jacques, “Optical properties of biological tissues: a review,” *Phys. Med. Biol.* **58**, R37–R61 (2013).
40. J. L. Sandell and T. C. Zhu, “A review of *in-vivo* optical properties of human tissues and its impact on PDT,” *J. Biophotonics* **4**(11–12), 773–787 (2011).
41. A. N. Bashkatov, E. A. Genina, and V. V. Tuchin, “Optical properties of skin, subcutaneous, and muscle tissues: a review,” *J. Innovative Opt. Health Sci.* **4**(1), 9–38 (2011).
42. T. Kono and J. Yamada, “*In vivo* measurement of optical properties of human skin for 450–800 nm and 950–1600 nm wavelengths,” *Int. J. Thermophys.* **40**(5), 51 (2019).
43. S.-H. Tseng, A. Grant, and A. Durkin, “*In vivo* determination of skin near-infrared optical properties using diffuse optical spectroscopy,” *J. Biomed. Opt.* **13**(1), 014016 (2008).
44. S. Tzoumas et al., “Eigenspectra optoacoustic tomography achieves quantitative blood oxygenation imaging deep in tissues,” *Nat. Commun.* **7**, 12121 (2016).
45. A. Hussain et al., “Photoacoustic and acousto-optic tomography for quantitative and functional imaging,” *Optica* **5**(12), 1579–1589 (2018).
46. J. Gröhl et al., “Estimation of blood oxygenation with learned spectral decoloring for quantitative photoacoustic imaging (LSD-qPAI),” arXiv:1902.05839 (15 February 2019).
47. J. Buchmann et al., “Three-dimensional quantitative photoacoustic tomography using an adjoint radiance Monte Carlo model and gradient descent,” *J. Biomed. Opt.* **24**(6), 066001 (2019).
48. G.-S. Jeng et al., “Real-time spectroscopic photoacoustic/ultrasound (PAUS) scanning with simultaneous fluence compensation and motion correction for quantitative molecular imaging,” bioRxiv 2019.12.20.885251 (23 December 2019).
49. M. Kim et al., “Fluence compensation for real-time spectroscopic photoacoustic imaging,” arXiv:2001.09572 (27 January 2019).

Leonie Ulrich received her BSc degree in physics from the University of Zurich, Switzerland, in 2013, and her MSc degree in physics from the University of Heidelberg, Germany, in 2016. Currently, she is a PhD student at the Institute of Applied Physics, University of Bern, Switzerland. Her research focuses on quantitative optoacoustic imaging and light propagation in scattering media.

Kai Gerrit Held received his MSc degree in biomedical engineering from the University of Twente, Enschede, The Netherlands, in 2013, and his PhD in physics from the University of Bern, Switzerland, in 2017. As a post-doctoral researcher at the University of Bern, he focused on quantitative *in vivo* imaging of blood oxygenation using a handheld system for combined optoacoustic and ultrasound imaging. In 2018, he joined ABB Corporate Research as a scientist.

Michael Jaeger studied physics in Bern, Switzerland, where he received his PhD in physics in 2007. In 2010/2011, he joined the ICR and RMH, Sutton, United Kingdom. In 2012, he won a career development grant from the Swiss National Science Foundation for developing handheld speed-of-sound tomography. Since then, he is a group leader at the Institute of Applied Physics, University of Bern. His research focuses on any ultrasound imaging methods.

Martin Frenz received his PhD in physics from the University of Bern, Switzerland, in 1990. In 1995, he joined the University of Texas in Austin, USA. Since 2002, he has been a professor and head of the Biomedical Photonics Department of the Institute of Applied Physics at the University of Bern, Switzerland, specializing on imaging modalities in biomedicine, including quantitative optoacoustic imaging and sensing and speed of sound imaging. He is a fellow of SPIE and ASLMS.

Hidayet Günhan Akarçay completed his MSc degree at the École Nationale Supérieure de Physique de Strasbourg, before joining the University of Bern, Switzerland, to work on his PhD until 2012. He then worked as a postdoctoral fellow in Montreal, Canada, and Ulm, Germany (2012 to 2013). He is currently leader of the Light Propagation in Biomedical Applications Group at the IAP. His work focuses on the numerical modeling of polarized light propagation in condensed soft matter.